A kinematic subgrid scale model for large-eddy simulation of turbulence-generated sound

Hua-Dong Yao [a]; Guo-Wei He [a]

[a] Chinese Academy of Sciences, LNM, Institute of Mechanics, Beijing, P. R. China

PLEASE SCROLL DOWN FOR ARTICLE

Taylor & Francis
Taylor & Francis Group

A kinematic subgrid scale model for large-eddy simulation of turbulence-generated sound

Hua-Dong Yao and Guo-Wei He*

LNM, Institute of Mechanics, Chinese Academy of Sciences, Beijing 100080, P. R. China

In the hybrid approach of large-eddy simulation (LES) and Lighthill's acoustic analogy for turbulence-generated sound, the turbulence source fields are obtained using an LES and the turbulence-generated sound at far fields is calculated from Lighthill's acoustic analogy. As only the velocity fields at resolved scales are available from the LES, the Lighthill stress tensor, serving as a source term in Lighthill's acoustic equation, has to be evaluated from the resolved velocity fields. As a result, the contribution from the unresolved velocity fields is missing in the conventional LES. The sound of missing scales is shown to be important and hence needs to be modeled. The present study proposes a kinematic subgrid-scale (SGS) model which recasts the unresolved velocity fields into Lighthill's stress tensors. A kinematic simulation is used to construct the unresolved velocity fields with the imposed temporal statistics, which is consistent with the random sweeping hypothesis. The kinematic SGS model is used to calculate sound power spectra from isotropic turbulence and yields an improved result: the missing portion of the sound power spectra is approximately recovered in the LES.

Keywords: large-eddy simulation; turbulence-generated sound; kinematic simulation

1. Introduction

The numerical prediction of the sound radiated from turbulent flows is a challenge problem for computational fluid dynamics. Recently, a hybrid approach of large-eddy simulation (LES) and Lighthill's acoustic analogy has been developed for this problem. In the hybrid approach [1], the computation of turbulent flows is decoupled from the computation of the noise: the Navier–Stokes equations are solved using an LES and the Lighthill's acoustic equation is numerically integrated. As only the velocity fields at resolved scales are available from LES, the Lighthill stress tensor, serving as a source term in Lighthill's acoustic equation, has to be evaluated from the resolved velocity fields, and thus a subgrid-scale (SGS) model for the Lighthill stress tensor is needed. The objective of this study is to develop a kinematic SGS model for the Lighthill stress tensor in the hybrid approach.

To understand this problem, we decompose the simplest form of Lighthill's stress tensors in incompressible flows into the following three components [1,2]:

$$T_{ij} = \underbrace{\rho_0 \overline{u}_i \overline{u}_j}_{\text{Resolved stress}} + \underbrace{\rho_0 (\overline{u_i u_j} - \overline{u}_i \overline{u}_j)}_{\text{SGS residual stress}} + \underbrace{\rho_0 (u_i u_j - \overline{u_i u_j})}_{\text{Unresolved stress}} \tag{1}$$

*Corresponding author. E-mail: hgw@lnm.imech.ac.cn or guoweihe@yahoo.com

where the overbar denotes a spatial filtering and ρ_0 a constant density. In Equation (1), the first term represents the resolved stress tensor, which can be directly calculated from LES; the second term represents an SGS residual stress tensor, which can be modeled using the resolved velocity fields in LES; and the third term represents an unresolved stress tensor, which is completely missing in LES. In the recent assessments of LES-based sound radiation calculation, Seror et al. [2] found that the SGS residual stress cannot be neglected and thus an SGS model is required to recover its contributions to acoustic fields. In their calculation, the scale-similarity SGS model is used for this purpose and yields better results than the eddy-viscosity-type SGS models. Bodony and Lele [3,4] indicate that high-frequency spectral components in jet noise are highly annoying to the ear and heavily weighted in noise regulation. These components are associated with the unresolved stresses at missing scales and are not captured by the current LES grid. Therefore, an SGS noise model of missing scales is important and needs to be developed.

A turbulent velocity field can be decomposed into a resolved part and an unresolved one, using a filtering operator, such as

$$\boldsymbol{u} = \bar{\boldsymbol{u}} + \boldsymbol{u}', \tag{2}$$

where $\bar{\boldsymbol{u}}$ is a resolved velocity field and $\boldsymbol{u}'$ an unresolved one. In LES, the resolved velocity $\bar{\boldsymbol{u}}$ is explicitly computed and the effect of the unresolved velocity $\boldsymbol{u}'$ on the resolved one $\bar{\boldsymbol{u}}$ is modeled. Many SGS models, such as the eddy-viscosity-type SGS models, have been developed for this purpose [5]. However, in such a problem as turbulence-generated sound, the unresolved velocity is essentially important to the sound in far fields by itself and its function cannot be represented by the currently existing SGS models for the SGS residual stress. Therefore, we propose to use a kinematic simulation (KS) to explicitly construct the unresolved velocity fields with the required statistic properties in both space and time. Kinematic simulation [6] is an approach to synthesize turbulent flows without explicitly solving the Navier–Stokes equations. This approach has been used to simulate turbulent dispersion [7] and turbulence noise [8,9] among others. The new development in this paper is to apply KS only to the unresolved velocity fields, with the required time correlations. This requirement is consistent with the random sweeping hypothesis [10,11] and guarantees that the synthesized velocity field at the unresolved scales has the space–time correlations consistent with the resolved velocity fields in LES. The KS serves as an SGS model to represent the velocity fields at unresolved scales. Accordingly, it will be referred to as a kinematic SGS model or simply a KS SGS model. This paper is organized as follows: In Section 2, the hybrid approach of LES and Lighthill's acoustic analogy is introduced. The kinematic SGS model is developed in Section 3. The numerical computation and results are presented in Section 4, and the discussion and conclusions in Section 5.

2.   A hybrid approach of LES and Lighthill's acoustic analogy

We consider the far-field sound generated by isotropic turbulence. In spirit of Lighthill's analogy [12], the acoustic source field can be obtained from an incompressible flow approximation. Thus, the flow in the near field is governed by the Navier–Stokes equations

$$\frac{\partial u_i}{\partial x_i} = 0, \quad \frac{\partial u_i}{\partial t} + u_j \frac{\partial u_i}{\partial x_j} = -\frac{\partial p}{\partial x_i} + \frac{1}{Re} \frac{\partial^2 u_i}{\partial x_j x_j}. \tag{3}$$

Here, all variables are dimensionless, with the velocity normalized by a reference velocity U_{ref}, pressure by $\rho_0 U_{\text{ref}}^2$, spatial coordinates by a reference length scale L_{ref} and time by

$L_{\mathrm{ref}}/U_{\mathrm{ref}}$. The density fluctuation due to acoustic wave propagation from the turbulence source region is governed by the Lighthill acoustic equation. In order to be consistent with the previous paper [11], we write down the Lighthill acoustic equation in the dimensional form

$$\frac{\partial^2 \rho}{\partial t^2} - c_0^2 \nabla^2 \rho = \frac{\partial^2 T_{ij}}{\partial x_i \partial x_j}, \tag{4}$$

where

$$T_{ij} = \rho u_i u_j + \left(p - c_0^2 \rho\right)\delta_{ij} - \tau_{ij} \tag{5}$$

is the Lighthill stress tensor dependent on the fluctuation velocity relative to the mean one. τ_{ij} is the viscous stress tensor. Under the assumptions of the isentropic acoustic pressure fluctuations at lower Mach number and high-Reynolds-number turbulent flows, the Lighthill tensor can be simplified to $T_{ij} = \rho u_i u_j$.

The acoustic field can be solved from the Lighthill acoustic equation. In the case of acoustic far field, the solution of the Lighthill acoustic equation can be expressed by [13]

$$\rho(\boldsymbol{x}, t) - \rho_0 = \frac{1}{4\pi c_0^2} \frac{x_i x_j}{x^3} \int \frac{\partial^2 T_{ij}}{\partial t^2}\left(\boldsymbol{y}, t - \frac{|\boldsymbol{x} - \boldsymbol{y}|}{c_0}\right) d^3 \boldsymbol{y}, \tag{6}$$

where $\boldsymbol{x}$ and $\boldsymbol{y}$ denote the position vectors of an observation point and a source element respectively. Accordingly, the radiated fluctuating acoustic pressure is $p(\boldsymbol{x}, t) - p_0 = c_0^2[\rho(\boldsymbol{x}, t) - \rho_0]$. Then, the acoustic power spectra can be calculated from

$$I(\omega) = \langle p(\boldsymbol{x}, \omega) p(\boldsymbol{x}, -\omega)\rangle / \rho_0 c_0. \tag{7}$$

When the direct numerical simulation (DNS) is used to solve the Navier–Stokes equations, the Lighthill stress tensor can be fully calculated and thus Equation (7) is used to predict the far-field sound. However, when LES is used to solve the Navier–Stokes equations, the resolved stress is the only one available from the LES. The SGS residual stress can be partially recovered using an SGS model but the unresolved stress is completely missing. The SGS residual stress and unresolved stress are mainly dependent on the unresolved velocity at missing scales. The unresolved velocity fields are associated with the high-frequency part of sound power spectra and cannot be represented by any surrogate at resolved scales. These considerations motivate the present research to synthesize an unresolved velocity field.

3. A kinematic SGS model

The kinematic SGS model is based on the KS approach [6] for isotropic turbulence, where the approach is designed to be applied only to unresolved velocity fields in LES. It provides the unresolved velocity fields with the space–time correlations consistent with the resolved velocity fields. In the present study, (1) the random sweeping hypothesis is used to determine the decorrelation timescales of the unresolved velocity fields; (2) the energy spectra at unresolved scales are extrapolated from the resolved velocity fields using a spectral model; (3) the wave numbers at unresolved scales are taken to be distributed in

a linear ratio. This is consistent with the DNS and the fast Fourier transformation (FFT) in the present simulation, which is different from the previous methods [6].

We propose to kinematically construct a turbulent velocity field at unresolved scales. The unresolved velocity field is obtained by a summation of Fourier modes with the wave numbers larger than the cutoff one k_c, with $|\mathbf{k}_{nm}| \geq k_c$:

$$u_i^{'}(\mathbf{x}, t) = \sum_{|n|=k_c}^{N} \sum_{m=1}^{M} \left[a_{inm} \cos(\mathbf{k}_{nm} \cdot \mathbf{x} + \omega_{nm}t) + b_{inm} \sin(\mathbf{k}_{nm} \cdot \mathbf{x} + \omega_{nm}t) \right]. \quad (8)$$

The *sin* and *cosine* expressions can be combined into a simple exponential form

$$u_i^{'}(\mathbf{x}, t) = \sum_{|n|=k_c}^{N} \sum_{m=1}^{M} c_{inm} \exp\left[i(\mathbf{k}_{nm} \cdot \mathbf{x} + \omega_{nm}t)\right] = \sum_{|n|=k_c}^{N} \sum_{m=1}^{M} \hat{u}_{inm}^{'}(\mathbf{k}_{nm}, t) \exp\left[i(\mathbf{k}_{nm} \cdot \mathbf{x})\right]. \quad (9)$$

Here, $\mathbf{k}_{nm}$ denotes the mth wave number vector on the nth wave shell with its magnitude $|\mathbf{k}_{nm}| = k_n$. The frequency ω_{nm} corresponds to the wave number vector $\mathbf{k}_{nm}$. $\hat{\mathbf{u}}_{nm}^{'}$ denotes the Fourier mode corresponding to the wave number vector $\mathbf{k}_{nm}$ with its ith component $\hat{u}_{inm}^{'}$. Similarly, the vectors $\mathbf{a}_{nm} = \{a_{inm}\}$, $\mathbf{b}_{nm} = \{b_{inm}\}$ and $\mathbf{c}_{nm} = \{c_{inm}\}$ correspond to the wave number vector $\mathbf{k}_{nm}$, such that

$$c_{inm} = \frac{a_{inm} - i b_{inm}}{2},$$

$$c_{i(-n)m} = \frac{a_{inm} + i b_{inm}}{2}. \quad (10)$$

As a result, we have the Fourier modes of the velocity components,

$$\hat{u}_{inm}^{'}(\mathbf{k}_{nm}, t) = c_{inm} \exp\left(i\omega_{nm}t\right). \quad (11)$$

If $M = 1$, Equation (9) is the one used in [6]. It is noted that $\mathbf{k}_{nm}$, a_{inm}, b_{inm} and ω_{nm} in Equation (9) need to be determined.

The wave number vector $\mathbf{k}_{nm}$ is taken to be randomly distributed on a spherical shell $|\mathbf{k}_{nm}| = k_n$, that is to say,

$$\mathbf{k}_{nm} = k_n \left(\sin\theta_m \cos\phi_m, \sin\theta_m \sin\phi_m, \cos\theta_m\right), \quad (12)$$

where the angles $\theta_m \in [0, 2\pi]$ and $\phi_m \in [0, \pi]$ are the random numbers of uniform distribution. Therefore, there are in total M wave vectors on each wave shell. In practice, M should be chosen to be appropriately large to ensure statistic convergence. To facilitate the discrete FFT package in the current numerical simulation, the wave vector magnitudes k_n are taken to be linearly distributed, such that

$$k_{n+1} = k_n + \delta k_n, \ k_n \in (k_c, k_{\max}), \ \delta k_n = 1, \quad (13)$$

where k_c is the cutoff wave number in LES and $k_{\max}$ is the maximum wave number in DNS.

The amplitude vectors $\boldsymbol{a}_{nm}$ and $\boldsymbol{b}_{nm}$ are taken as follows:

$$a_{inm} = \left(\delta_{ij} - \frac{k_{inm}k_{jnm}}{|\boldsymbol{k}_{nm}|^2} \right) a'_{jnm}, \tag{14}$$

$$b_{inm} = \left(\delta_{ij} - \frac{k_{inm}k_{jnm}}{|\boldsymbol{k}_{nm}|^2} \right) b'_{jnm}, \tag{15}$$

where

$$\boldsymbol{a}'_{nm} = A(\sin\theta'_m \cos\phi'_m, \sin\theta'_m \sin\phi'_m, \cos\theta'_m), \tag{16}$$

$$\boldsymbol{b}'_{n,m} = A(\sin\theta''_m \cos\phi''_m, \sin\theta''_m \sin\phi''_m, \cos\theta''_m). \tag{17}$$

Here, $\theta'_m, \theta''_m \in [0, 2\pi]$ and $\phi'_m, \phi''_m \in [0, \pi]$ are the uncorrelated random numbers of uniform distribution. Consequently, a'_{inm} and b'_{inm} are also uncorrelated with zero means. The constant A is given by

$$A = \langle |\boldsymbol{a}_{nm}|^2 \rangle = \langle |\boldsymbol{b}_{nm}|^2 \rangle = \frac{2}{M} E(k_n)\delta k_n. \tag{18}$$

It is easily verified that the velocity fields thus obtained satisfy the incompressible condition

$$\boldsymbol{a}_{nm} \cdot \boldsymbol{k}_{nm} = \boldsymbol{b}_{nm} \cdot \boldsymbol{k}_{nm} = 0. \tag{19}$$

The mode frequency ω_{nm} can be chosen such that the unresolved velocity field satisfies the random sweeping hypothesis. This suggests

$$\omega_{nm} = v_m k_n, \tag{20}$$

where the random variable v_m is normally distributed with zero mean and the variance being V. The variance V is the r.m.s. of fluctuating velocity at resolved scales. Furthermore, the random variable v_m is required to be uncorrelated with the amplitudes a_{inm} and b_{inm} and the wave number ω_{inm}.

One has to verify that this procedure could generate a turbulent field which features the required statistic properties. For example, we can calculate the time correlations of velocity modes

$$\langle \hat{u}'_{inm}(\boldsymbol{k}_{nm}, t)\hat{u}'_{inm}(-\boldsymbol{k}_{nm}, t + \tau) \rangle \delta k_n$$

$$= \langle \hat{u}'_{inm}(\boldsymbol{k}_{nm}, t)\hat{u}'_{inm}(-\boldsymbol{k}_{nm}, t) \rangle \langle \exp(i\,v_m k_n) \rangle \delta k_n$$

$$= \left[\sum_{i=1}^{3} \sum_{m=1}^{M} \frac{\langle a_{inm}^2 \rangle + \langle b_{inm}^2 \rangle}{4} \right] \exp\left(-\frac{1}{2}V^2 k_n^2 \tau^2 \right) \delta k_n$$

$$= E(k_n)\exp\left(-\frac{1}{2}V^2 k_n^2 \tau^2 \right). \tag{21}$$

As a result, the velocity field indeed exhibits the energy spectra $E(k_n)$ and the decorrelation timescale $(Vk_n)^{-1}$.

Table 1.   Relevant parameters and statistical quantities in DNS.

Case	Method	Nodes	k_c	Re_λ	u_{rms}	L	λ	ξ	CFL no.
1	DNS	512^3	170	206.58	0.810	1.469	0.238	1.432	0.208
2	LES	64^3	21						
3	LES	128^3	42						
4	LES	256^3	85						
5	LES+KS	64^3	21						
6	LES+KS	128^3	42						
7	LES+KS	256^3	85						

Note: Here k_c is the cutoff wave number, Re_λ the Taylor-scale Reynolds number, L the integral length scale, λ the Taylor microscale. $\xi = k_{\max}\eta$ indicates the spatial resolution; u_{rms} is the root-mean-square of velocity fluctuations.

4.   Numerical results

A test of the kinematic SGS model was carried out to determine the accuracy of the model in prediction of sound power spectra. The test was performed using the DNS database of isotropic turbulence. The DNS for isotropic turbulence was obtained using a pseudo-spectral method. The computational domain is a box of length 2π on each side, where the periodic boundary conditions are applied. To keep the turbulence stationary, an external force $f(k)$ is imposed on the first two shells of wave numbers $k = 1, 2$. Aliasing errors are removed through the two-thirds truncation rule. The Adams–Bashforth scheme is used for time advance. Five cases are run in the present study: Case 1 is the DNS with $Re_\lambda = 206.58$ on a 512^3 grid; Case 2, Case 3 and Case 4 are the LES on grid size 64^3, 128^3 and 256^3, respectively, without the kinematic SGS model; Case 5, Case 6 and Case 7 are the LES on the same grid size as Case 2, Case 3 and Case 4, respectively, using the kinematic SGS model. The relevant parameters for all cases are listed in Table 1.

In high-Reynolds-number turbulent flows, the high wave number portion of the energy spectra exhibits a universal form. The von Karman spectrum is a simple model for the universal form. We will use the von Karman spectrum to reconstruct the unresolved velocity fields in LES. The von Karman spectrum [14] has the general form of

$$E(k) = C\varepsilon^{2/3}k^{-5/3}\left(\frac{kL}{[(kL)^2 + c_L]^{1/2}}\right)^{5/3+p_0}\exp\left\{-\beta\left\{[(k\eta)^4 + c_\eta^4]^{1/4} - c_\eta\right\}\right\}, \quad (22)$$

where the constant $p_0 = 4$ is taken to ensure the energy spectrum $E(k)$ varying as k^4 for small wave numbers k; the constant $\beta = 5.2$ is determined by the experiment [15]; $c_L = 6.78$ and $c_\eta = 0.4$ are fixed by the turbulent kinetic energy and the energy dissipation rate. The remaining parameters are determined from the LES: $C = 1.5$ is taken to match the energy level; the integral length scale $L = 1.5\pi\langle u_i^2\rangle^{-1}\int_0^{k_c} k^{-1}E(k)dk$ and the dissipation length scale $\eta = (\nu/\epsilon)^{1/4}$, with $\epsilon = \delta E$ being the added energy at each time step [16].

Figure 1 shows the energy spectra from the DNS, the LES without the kinematic SGS model and the LES with the kinematic SGS model. The kinematic SGS model does extend the energy spectra from the maximum wave number of the LES to the maximum one of the DNS. The recovered energy spectra for the unresolved velocity fields become better closer to the DNS one as the cutoff wave number k_c is increased. However, the recovered portions still decay faster than those in the DNS, since the energy spectra in LES decay faster at larger resolved wave numbers than those in the DNS.
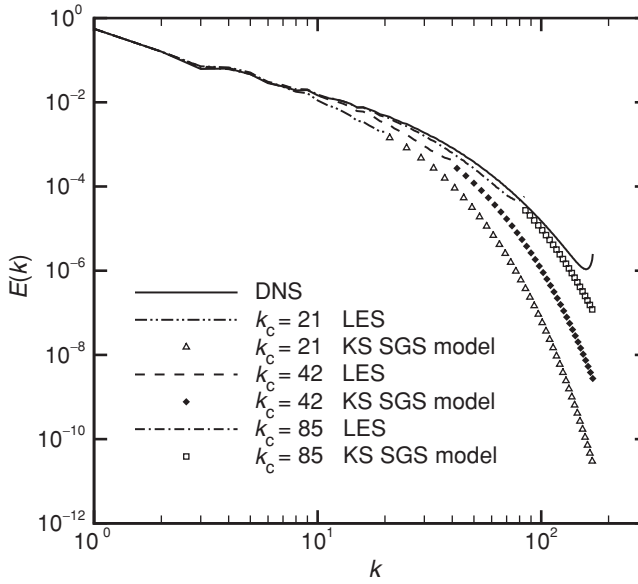
Figure 1. Energy spectra for the DNS on a 512^3 grid and the LES on three grids: 64^3, 128^3 and 256^3 with and without the kinematic SGS model.

4.1. *Time correlations*

The performance of the kinematic SGS model will be evaluated in terms of the time correlations. This can be achieved by comparing the time correlations from DNS with the ones from the LES with the kinematic SGS model. The random sweeping hypothesis implies that the decorrelation timescales of small-scale eddies are mainly determined by a sweeping velocity, which is the r.m.s. of fluctuating velocities. As a result, the time correlations of the DNS should collapse into one single curve with the time axis rescaled by the sweeping velocity. If the kinematic SGS model could generate an unresolved velocity field with the correct timescales, the time correlations of velocity modes at both resolved and unresolved scales should collapse together. Therefore, we can evaluate the performance of the kinematic SGS model in terms of (1) the collapse of the time correlations of velocity modes in the LES with the ones from the KS SGS model and (2) the approximation of collapsed curves from LES to the ones from DNS.

The normalized time correlation coefficients can be calculated as follows:

$$
\begin{aligned}
C_u(k_n, \tau) &= \frac{\langle \hat{u}_i(\boldsymbol{k}_{n,m}, t)\hat{u}_i(-\boldsymbol{k}_{n,m}, t+\tau)\rangle}{\langle \hat{u}_i(\boldsymbol{k}_{n,m}, t)\hat{u}_i(-\boldsymbol{k}_{n,m}, t)\rangle} \\
&= \frac{\langle \hat{u}_{inm}(\boldsymbol{k}_{nm}, t)\hat{u}_{inm}(-\boldsymbol{k}_{nm}, t+\tau)\rangle}{\langle \hat{u}_{inm}(\boldsymbol{k}_{nm}, t)\hat{u}_{inm}(-\boldsymbol{k}_{nm}, t)\rangle},
\end{aligned}
\tag{23}
$$

where the ensemble average is performed over the wave number shell $k = |\boldsymbol{k}|$ and the different start times. The number of modes at each wave shell should be large enough to suppress statistic errors. For example, $M = 40,000$ for Case 5 and Case 6 and $M = 4000$ for Case 7. The start time t in Equation (23) is chosen from 0.0 to 2.0 eddy turnover time with an increment of 0.25. According to the random sweeping hypothesis, the sweeping
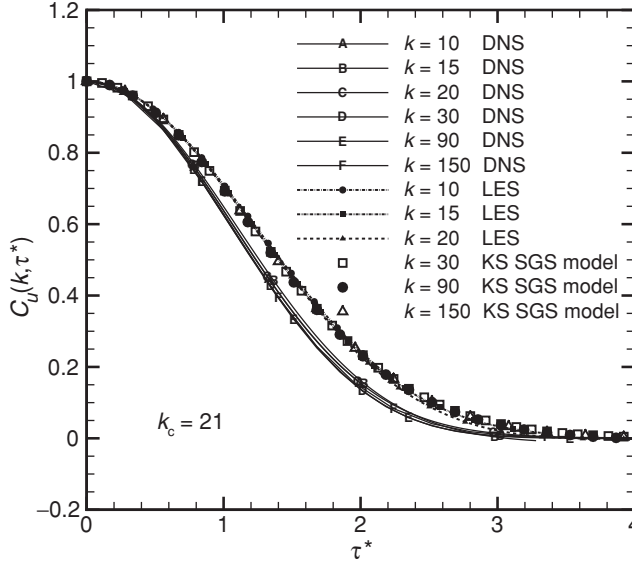
Figure 2.   Time correlations vs time lag normalized by the sweeping velocity. The curves with letters are from the DNS, the curves with symbols from the LES and the symbols from the LES with the kinematic SGS model. The DNS is performed on a 512^3 grid and the LES on a 64^3 grid.

velocity is the r.m.s. of the fluctuating velocity. Therefore, the sweeping velocity in the KS SGS model is approximately the square root of total energy in LES. Alternatively, the sweeping velocity can be taken as the average of the decorrelation timescales of the mode correlations at resolved scales in LES.

Figure 2 plots the time correlations of velocity modes for $k = 10, 15, 20, 30, 90$ and 150 from Case 1, Case 2 and Case 5. The time separations here are rescaled using the different sweeping velocities in DNS and LES respectively. It is observed that the time correlations from Case 3 and Case 5 collapse into one curve, which verifies that the velocity modes from the kinematic SGS model share the same decorrelation timescales with the ones from the LES. The time correlations in the DNS also collapse into one single curve as shown in Figure 2. It is easily seen that the collapsed curves in LES are virtually close to the ones in DNS with a slightly slower decay, since the sweeping velocity in DNS is slightly larger than the one in LES.

Figures 3 and 4 display the mode correlations versus the rescaled time separation in DNS and LES on the 128^3 and 256^3 grids, respectively. Again, the mode correlations from the LES and kinematic SGS model collapse into one single curve while the mode correlations from the DNS collapse into another one. Although the collapsed curves from the LES and kinematic SGS model decay slower than the ones from DNS, their differences are very small. The LES becomes better as the resolution in LES is increased.

4.2.   *Sound power spectra*

The intensity of a sound radiation is usually measured by sound power spectra, defined as a Fourier transformation of pressure correlation in time. A brute-force calculation of sound power spectra using DNS data needs a large amount of samples [17,18], which is not easily obtained from the current simulation. One solution is to perform the ensemble average over
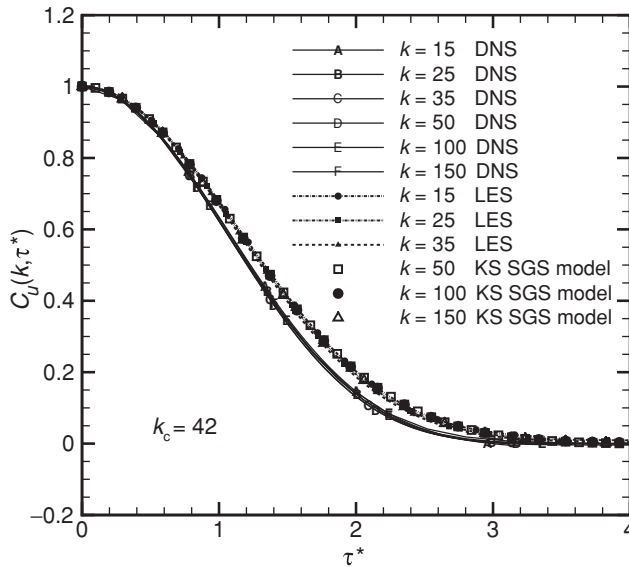
Figure 3. Time correlations vs time lag normalized by the sweeping velocity. The curves with letters are from the DNS, the curves with symbols from the LES and the symbols from the LES with the kinematic SGS model. The DNS is performed on a 512^3 grid and the LES on a 128^3 grid.

different observation points. It is known [19] that, at the boundary of computation domain, the sudden termination of the Lighthill stress terms may cause strongly spurious noise. This requires that the observation points should be symmetric about the computational domain, so that the spurious noise can be canceled with each other [2,20,21]. However, this is not possible for the present simulation of isotropic turbulence, where the computational domain
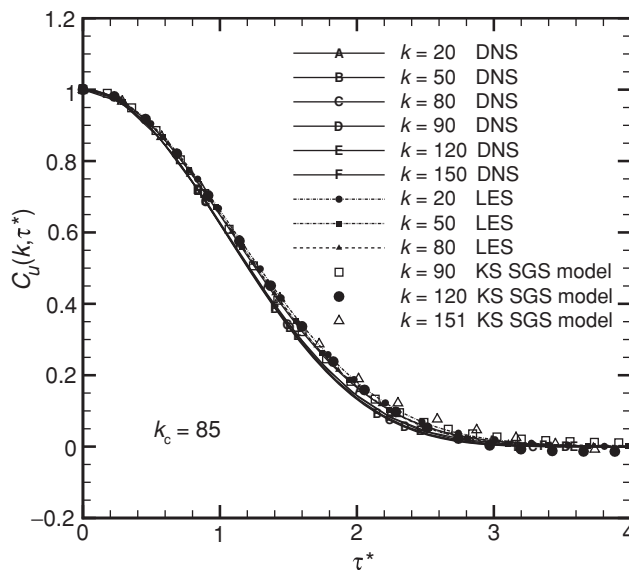

Figure 4. Time correlations vs time lag normalized by the sweeping velocity. The curves with letters are from the DNS, the curves with symbols from the LES and the symbols from the LES with the kinematic SGS model. The DNS is performed on a 512^3 grid and the LES on a 256^3 grid.

is a box without sufficiently symmetric observation points available. Another solution is to make a correction using the Taylor frozen flow hypothesis [19]. However, for isotropic turbulence, the Taylor frozen flow hypothesis is not valid.

Proudman's classic analysis [22] yields an analytical expression for the sound power spectra at far fields. This expression relates the sound power spectra to the space–time correlations of fluctuating velocities, where the quasi-normality assumption is used. The quasi-normality assumption breaks up a quadruple correlation into the product of the double correlations in space and time. It is shown that the quasi-normality assumption is a satisfactory approximation in isotropic turbulence. Rubinstein and Zhou [23] further simplify Proudman's expression using the compact source assumption, which gives

$$I(\omega) = \frac{2\rho_0\omega^4}{15\pi c_0^5} \int_0^{+\infty} \frac{E^2(k)}{k^2}\hat{c}(k,\omega)dk. \qquad (24)$$

Here, $\hat{c}(k,\omega)$ is the Fourier transformation of the squared space–time correlation $c^2(k,\tau)$, given by

$$\hat{c}(k,\omega) = \int_{-\infty}^{+\infty} c^2(k,\tau)e^{-i\omega\tau}d\tau, \qquad (25)$$

where $c(k,\tau)$ is the time correlations of velocity modes without normalization, different from the normalized correlations shown in Equation (23). A separation of the contribution of resolved velocity from the one of the unresolved velocity leads to

$$I(\omega) = \frac{2\rho_0\omega^4}{15\pi c_0^5} \left(\int_{k_{\min}}^{k_c} \frac{E^2(k)}{k^2}\hat{c}(k,\omega)dk + \int_{k_c}^{k_{\max}} \frac{E^2(k)}{k^2}\hat{c}(k,\omega)dk \right), \qquad (26)$$

where $k_{\min}$ is the minimum wave number and $k_{\max}$ the maximum wave number in the DNS. k_c is the cutoff wave number in the LES. The second term in the bracket is computed by the KS SGS model, and thus it vanishes in the DNS, or $k_c = k_{\max}$. The stationary isotropic turbulence is sustained by freezing the kinetic energy at the first two wave numbers. Hence, the artificial forcing may influence the fluctuating velocity at small wave numbers at moderate Reynolds numbers. For the sake of avoiding the artificial contamination, the lower limit of the first integral in Equation (26) is taken to be larger than 2, such as $k_{\min} = 4$.

We will use the time correlation of velocity mode to calculate the sound power spectra in terms of Equation (26). Each term in the expression can be accordingly calculated from the DNS and two LES with and without the KS SGS model. Here, the time correlations are calculated using the ensemble average over wave shells and the results obtained are shown to be accurate as in the previous subsection.

Figure 5 plots the sound power spectra calculated from the DNS on a 512^3 grid and the LES on three grids: 64^3, 128^3 and 256^3. It is observed that the LES under-predicts the sound power spectra at moderate frequencies and attenuates the sound power spectra at high frequencies, while it predicts the part at low frequencies well. Increasing grid improves the prediction of LES on sound power spectra. It suggests that the missing scales have important contributions to the sound power spectra at moderate and high frequencies. These results are in agreement with previous observations such as [2,11,24].

Figure 6 shows the comparisons between the sound power spectra obtained from the DNS on a 512^3 grid and two LES on a coarse grid size 64^3 with and without the kinematic
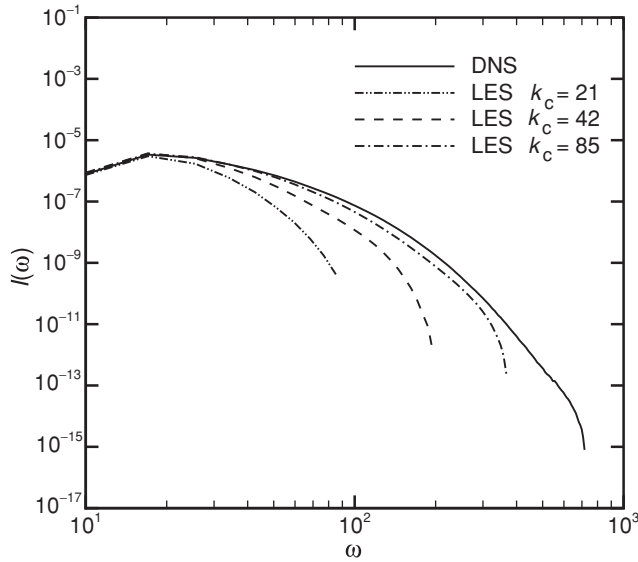
Figure 5. Sound power spectra from the DNS on a 512^3 grid and the LES on three grids: 64^3 ($k_c = 21$), 128^3 ($k_c = 42$) and 256^3 ($k_c = 85$).

SGS model. The sound power spectrum from the LES with the kinematic SGS model is closer to the one from the DNS than the LES without the kinematic SGS model at moderate frequencies. Moreover, the KS SGS model recovers the sound power spectra at high frequencies, which is completely missing in the LES without the kinematic SGS model. However, there still exist some differences between the DNS and the LES. That is
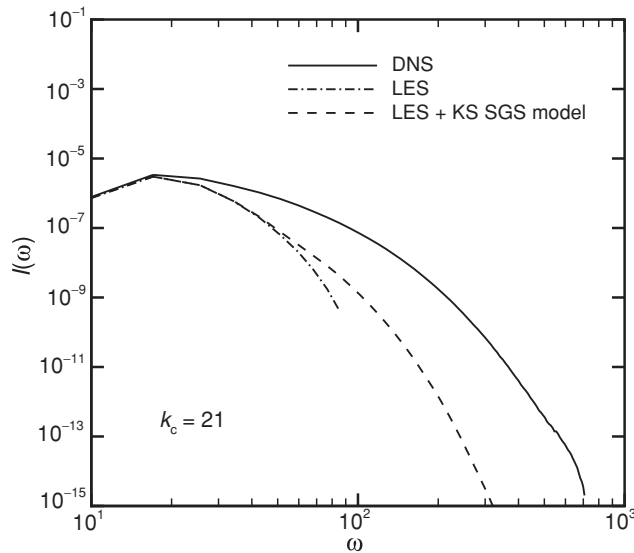

Figure 6. Sound power spectra from the DNS on a 512^3 grid and the LES on a 64^3 grid ($k_c = 21$) with and without the KS SGS model.
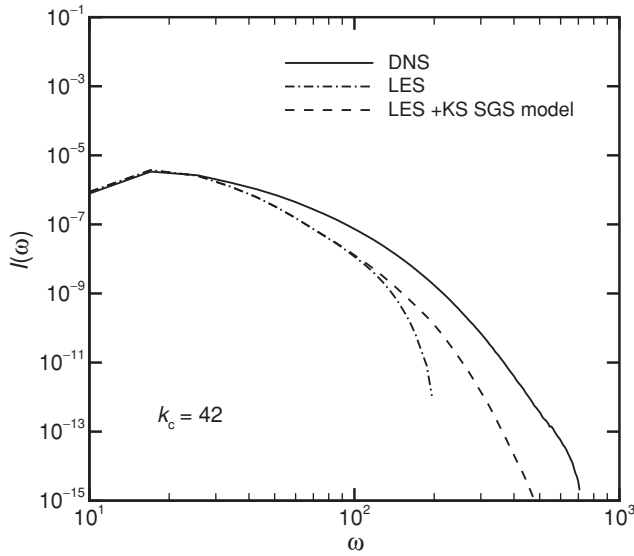
Figure 7.   Sound power spectra from the DNS on a 512^3 grid and the LES on a 128^3 grid ($k_c = 42$) with and without the KS SGS model.

because the grid ratio of the LES to the DNS here is 1:8, where the resolution in the LES is much lower than the one in the DNS.

   Figure 7 displays the sound power spectra from the DNS on a 512^3 grid and two LES on a 128^3 grid with and without the kinematic SGS model. The LES with the kinematic SGS model does improve the prediction of the sound power spectra at moderate frequencies and
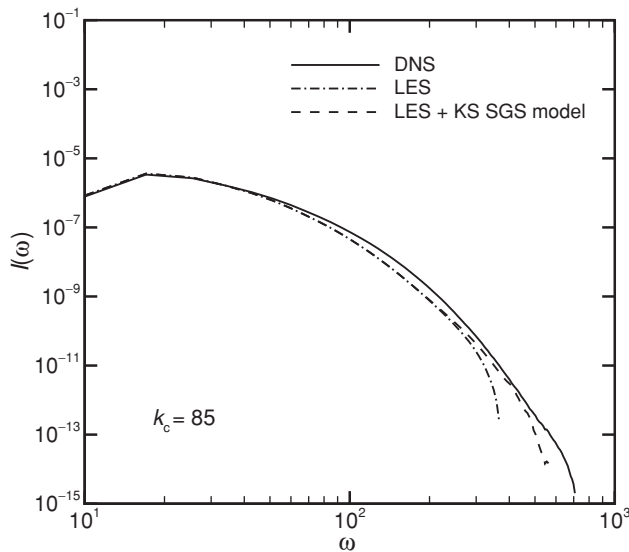

Figure 8.   Sound power spectra from the DNS on a 512^3 grid and the LES on a 256^3 grid ($k_c = 85$) with and without the KS SGS model.

better recovers the sound power spectra at high frequencies. The grid ratio here is 1:4. The discrepancies between the 128^3 LES and the DNS are less than the one between the 64^3 LES and the DNS. The LES with kinematic SGS model yields a reasonable approximation to the DNS result.

Figure 8 compares the sound power spectra from the DNS on a 512^3 grid with the one from the LES on a 256^3 grid with and without the kinematic SGS model. The results from the LES with the kinematic SGS model almost match those from the DNS, while the LES without the kinematic SGS model misses the portion of sound power spectra at higher frequencies. Therefore, the kinematic SGS model does recover the sound component at missing scales, even though a high resolution is used in the present LES.

5. Discussions and conclusions

The present work develops a kinematic SGS model, which reconstructs a random velocity field as an approximation to the unresolved velocity field in LES, using the KS approach. The random velocity field is reconstructed to be consistent with the required space–time correlations: an extrapolation of the energy spectrum of the resolved velocity in LES using the von Karman energy spectrum, and an imposition of the time correlations of the velocity modes using the sweeping velocity in LES. The velocity field is the sum of the resolved velocity in LES and the random velocity field obtained from the kinematic SGS model. They are used to evaluate the Lighthill stress tensor in the hybrid approach of LES and Lighthill's acoustic analogy. Comparison between the DNS and the LES with the kinematic SGS model indicates that the latter can predict the low-frequency spectra and approximately recover the high-frequency spectra, which is missing in the conventional LES without the kinematic SGS model.

It is possible to extend the kinematic SGS model to more complex flows that include shear effects and nonperiodic boundary conditions: (1) The random sweeping hypothesis used in the present kinematic SGS model is not suitable for turbulent shear flows, where shear adds another timescale to the unresolved velocity fields in addition to the sweeping velocity. The recently developed elliptic model [25] may be appropriate to incorporate the unsteadiness of the resolved velocity into the unresolved ones in LES; (2) The Fourier representation used in the present kinematic SGS model is not suitable for a nonperiodic boundary condition. A new representation for the random velocity fields in nonperiodic domains needs to be found for the unresolved velocity fields, such as wavelet functions.

References

[1] M. Wang, J.B. Freund, and S.K. Lele, *Computational prediction of flow-generated sound*, Ann. Rev. Fluid. Mech. 38 (2006), pp. 483–512.

[2] C. Seror, P. Sagaut, C. Bailly, and D. Juvé, *On the radiated noise computed by large-eddy simulation*, Phys. Fluids 13 (2001), pp. 476–487.

[3] D.J. Bodony and S.K. Lele, *A stochastic subgrid scale noise model for noise predictions of subsonic jets*, AIAA Paper 2003-3252, Presented at the 9th AIAA/CEAS Aeroacoustics Conference, Hilton Head, SC, 2003.

[4] D.J. Bodony and S.K. Lele, *On using large-eddy simulation for the prediction of noise from cold and heated turbulent jets*, Phys. Fluids 17 (2005), 085103.

[5] G.W. He, R. Rubinstein, and L.P. Wang, *Effects of subgrid-scale modeling on time correlations in large eddy simulation*, Phys. Fluids 14 (2002), pp. 2186–2193.

[6] J.C.H. Fung, J.C.R. Hunt, N.A. Malik, and R.J. Perkins, *Kinematic simulation of homogeneous turbulence by unsteady random Fourier modes*, J. Fluid Mech. 236 (1992), pp. 281–318.

[7] J.C.H. Fung and J.C. Vassilicos, *Two-particle dispersion in turbulentlike flows*, Phy. Rev. E 57 (1998), pp. 1677–1690.

[8] W. Bechara, C. Bailly, and P. Lafon, *Stochastic approach to noise modeling for free turbulent flows*, AIAA J. 32 (1994), pp. 455–463.

[9] B. Favier, F.S. Godeferd, and C. Cambon, *Modeling the far-field acoustic emission of rotating turbulence*, J. Turbulence 9 (2008), pp. 1–21.

[10] R.H. Kraichnan, *Kolmogorov's hypotheses and Eulerian turbulence theory*, Phys. Fluids 7 (1964), pp. 1723–1724.

[11] G.W. He, M. Wang, and S.K. Lele, *On the computation of space-time correlations by large-eddy simulation*, Phys. Fluids 16 (2004), pp. 3859–3867.

[12] M.J. Lighthill, *On sound generated aerodynamically: I. General theory*, Proc. R. Soc. Lond., Ser. A 211 (1952), pp. 564–587.

[13] M.E. Goldstein, *Aeroacoustics*, McGraw-Hill, New York, 1976.

[14] S.B. Pope, *Turbulent Flows*, Cambridge University Press, Cambridge, UK, 2000.

[15] S.G. Saddoughi and S.V. Veeravalli, *Local isotropy in turbulent boundary layers at high Reynolds number*, J. Fluid Mech. 268 (1994), pp. 333–372.

[16] P. Flohr and J.C. Vassilicos, *A scalar subgrid model with flow structure for large-eddy simulation of scalar variance*, J. Fluid Mech. 407 (2000), pp. 315–349.

[17] G.M. Lilley, *The radiated noise from isotropic turbulence*, Theor. Comput. Fluid Dyn. 6 (1994), pp. 281–301.

[18] G.M. Lilley, *The acoustic spectrum in the sound field of isotropic turbulence*, Int. J. Aeroacoust. 4 (2005), pp. 11–19.

[19] M. Wang, S.K. lele, and P. Moin, *Computation of quadruple noise using acoustic analogy*, AIAA J. 34 (1996), pp. 2247–2254.

[20] A. Witkowska, D. Juvé, and J.M. Brasseur, *Numerical study of noise from isotropic turbulence*, J. Comput. Acoust. 5 (1997), pp. 317–336.

[21] C. Seror, P. Sagaut, C. Bailly, and D. Juvé, *Sub-grid scale contributions to noise prediction in decaying turbulence*, AIAA J. 38 (2000), pp. 1795–1803.

[22] I. Proudman, *The generation of sound by isotropic turbulence*, Proc. R. Soc. Lond., Ser. A 214 (1952), pp. 119–132.

[23] R. Rubinstein and Y. Zhou, *The frequency spectrum of sound radiated by isotropic turbulence*, Phys. Lett. A 267 (2000), pp. 379–383.

[24] R. Rubinstein and Y. Zhou, *Characterization of sound radiation by unresolved scales of motion in computational aeroacoustics*, Eur. J. Mech. B/Fluids 21 (2002), pp. 105–110.

[25] G.-W. He and J.B. Zhang, *Elliptic model for space–time correlations in turbulent shear flows*, Phys. Rev. E 73 (2006), 055303-14.